Design and Verification of a Linear Parameter Varying Control Law for a Transport Aircraft

Christian Weiser, Daniel Ossmann, Richard Kuchar, Gertjan Looye

Abstract This paper presents the design, implementation and simulator verification of inner loop control laws based on linear parameter varying controller design techniques for a CS-25 certified fly-by-wire test aircraft. The synthesis method provides, in contrast to standard gain scheduling techniques, stability and robustness guarantees over the whole defined parameter envelope. Furthermore, it includes the design of the scheduling already in the synthesis process and avoids its a posteriori design. For the controller design, grid based linear parameter varying models of the longitudinal and lateral motion of the aircraft are generated. The longitudinal motion is augmented with two different reference tracking modes: load-factor and pitch rate command. The two control laws are compared in flight by the pilot to validate the handling qualities. The lateral motion control law features a rate command / attitude hold behavior, similar to schemes commonly used in fly-by-wire transport aircraft. Results from a simulation based verification campaign using DLR's 6 degree of freedom Robotic Motion Simulator are presented as final results in this paper. The simulator verification was conducted as preparation for flight tests of the designed control laws on a Cessna Citation II (550) aircraft.

1 Introduction

The design of flight control laws for transport aircraft is still mostly relying on classical control methods, such as proportional-integral-derivative controllers in combination with straightforward gain scheduling. Purpose of this work is the application of modern, robust control methods to a large transport aircraft. One modern control design technique which showed already promising results in flight is linear parameter varying (LPV) control [11], [12]. In addition to robustness against model

Christian Weiser, Daniel Ossmann, Richard Kuchar, Gertjan Looye
German Aerospace Center, Institute of System Dynamics and Control, Münchener Straße 20, 82234 Wessling, Germany, e-mail: `christian.weiser@dlr.de`

uncertainties, the LPV technique results in a controller which is already scheduled over flight envelope parameters [1]. Moreover, the LPV design can be seen as an extension to a previously conducted H_∞ control test campaign conducted with an unmanned aerial vehicle [20]. For this work, a CS 25 certified Cessna Citation II is chosen. On this aircraft, extensive experience of testing different fly-by-wire control laws has been gained within previous test campaigns for (Incremental) non-Linear Dynamic Inversion ((I)NDI) control [6]. Thus, the aircraft is a perfect test bed to develop new control algorithms on real aircraft.

The contribution of this paper is the development of an LPV control design for a Cessna Citation II aircraft. Therefore, LPV control for both axes is assessed within this work and validated during flight test by the pilot. LPV controller synthesis is employed to derive robust and scheduled control laws for both longitudinal and lateral augmentation of the test aircraft. The LPV technique is an advancement of classical robust control approaches and therefore allows achieving satisfactory robustness against model uncertainties via the closed loop shaping technique. Sufficient robustness with respect to model uncertainties and variations in the weight and balance configuration is considered in the control design. Moreover, the additional performance objectives defined herein are satisfactory handling qualities for augmented flight.

Within this work, a set of different command variables is selected and tested within DLR's 6 degree of freedom (DOF) Robotic Motion Simulator (RMS) framework in preparation for flight testing on-board the research aircraft. Firstly, an overview of the used means of LPV controller synthesis is given in Sect. 2. For the design of the control laws, an LPV representation of the nonlinear aircraft model of the Citation II is obtained within Sect. 3. Following, an LPV controller is developed based on the gridded LPV model obtained. Sect. 4 shows the results of non-linear simulations carried out with the derived control laws on a motion simulator platform.

2 LPV Control Design

In this section, the LPV approach used for control design is described. As specifications on the longitudinal and lateral flying qualities are given in [18] in the frequency domain, H_∞ control [17] is a useful method as it allows to 'shape' the closed loop frequency response. As extension to this, LPV control synthesis permits to use a similar scheme for LPV models [13], [21]. As a big advantage of the resulting controller it is directly scheduled with the defined varying parameter and guarantees stability and performance for all trajectories in ρ within the defined rate of change. Firstly, LPV models are introduced in (1) similar to Linear Time Invariant (LTI) models with the addition that all four matrices are dependent on a scheduling parameter ρ, which can vary over time.

$$G_\rho : \begin{cases} \dot{x}(t) = A(\rho(t))x(t) + B(\rho(t))u(t) \\ y(t) = C(\rho(t))x(t) + D(\rho(t))u(t) \end{cases} \tag{1}$$

To explain the idea of LPV control, the induced L_2 norm of an LPV system G_ρ from input d to output z over all allowed trajectories in a set P is defined as

$$\|G_\rho\|_\infty = \sup_{d \in L_2 \backslash 0 \rho \in P} \frac{\|z\|_2}{\|d\|_2} \tag{2}$$

Therefore, the induced L_2 norm measures the maximum gain of G_ρ, which is equivalent to the largest gain on L_2 input signals over all frequencies and input-output directions. For the design of linear parameter varying control laws, a closed loop interconnection including a weighting structure as seen in Fig. 1 is introduced in order to shape the closed loop response of the system. In the generalized plant of Fig. 1 the inputs are the reference signal r, the input disturbance d_i, and the output disturbance d_o. Outputs are the weighted tracking error $e = r\,[W_h \quad \underline{0}] - y$, as there is in most cases one reference signal and multiple measurement signals, and the weighted control effort u. This generic structure serves as base for both the longitudinal and lateral axis. The resulting input-output map for the control design is given by

$$\begin{bmatrix} z_e \\ z_u \end{bmatrix} = \begin{bmatrix} W_e & 0 \\ 0 & W_u \end{bmatrix} \begin{bmatrix} [W_h \quad \underline{0}]^T - S_\rho G_\rho K_{r,\rho} & -S_\rho G_\rho & S_\rho \\ S_{i,\rho}K_{r,\rho} & -T_{i,\rho} & K_{y,\rho}S_\rho \end{bmatrix} \begin{bmatrix} 1 & 0 & 0 \\ 0 & W_{d_i} & 0 \\ 0 & 0 & W_{d_o} \end{bmatrix} \begin{bmatrix} r \\ d_i \\ d_o \end{bmatrix}. \tag{3}$$

In (3) $K_{y,\rho}$ is the feedback part and $K_{r,\rho}$ the feed-forward part of the controller,
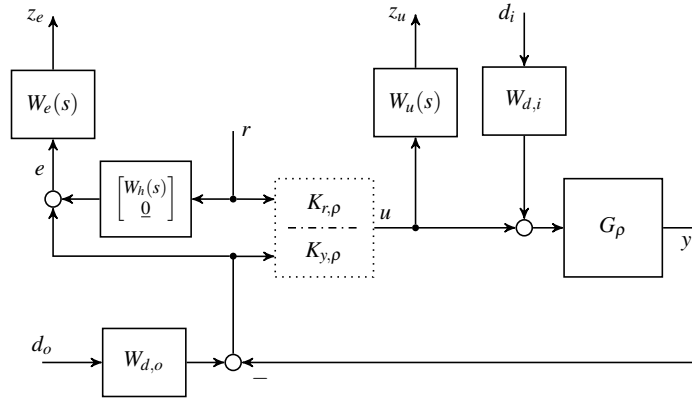
Fig. 1 Generic weighting structure used for the longitudinal and lateral controller design

G_ρ is the transfer matrix from command inputs to plant outputs. Further, $S_\rho = (I + G_\rho K_{y,\rho})^{-1}$ is the sensitivity function, and $S_{i,\rho} = (I + K_{y,\rho}G_\rho)^{-1}$ and $T_{i,\rho} = K_{y,\rho}G_\rho(I + K_\rho G_\rho)^{-1}$ are the input sensitivity and input complementary sensitivity

function, respectively $T_{r,\rho} = K_{r,\rho} G_\rho S_\rho$ complimentary sensitivity on reference signal. $W_e(s)$ and $W_u(s)$ are the diagonal output weighting matrices, and W_{d_i} and W_{d_o} are the diagonal input weighting matrices to be chosen in the design process. Note that the aircraft models G_ρ are scaled as proposed in [17] by input-output scaling. As indicated in Fig. 1, $W_e(s)$, $W_h(s)$ and $W_u(s)$ are selected as dynamic filters, while all other filters are constant. $W_h(s)$ denotes a handling quality filter in the form of eq. 4 and allows setting a design response in terms frequency ω_h and damping ζ_h.

$$W_h = \frac{\omega_h^2}{s^2 + \omega_h \zeta_h s + \omega_h^2}. \tag{4}$$

The entries for the shaping filter W_u are selected as first-order transfer functions with unit gain up to the available bandwidths $\omega_{a,i}$ for $i = 1, \ldots, n$ of each control input and approximately differentiating behavior beyond that frequency. In W_e only the first element is dynamic in order to weight the tracking behavior, while all other channels are set to constant values to weight the outputs. As in this paper integral behavior is demanded in the tracking channel, the choice for the first entry is a first-order transfer function with approximately integral behavior up to the desired bandwidth ω_b, which reduces the sensitivity up to this selected bandwidth. The weighting filters are selected so that the general design goals for pitch and roll control, which are taken from the [18] level 1 flying qualities specifications will be met. The demands for the flying qualities are defined in frequency domain for both longitudinal and lateral motion. For example, for design of the weighting filters of the pitch controller the control anticipation parameter (CAP) is used as a design parameter and sets a desired Short Period (SP) frequency. A more detailed description can be found in Sect. 3.2. Further, the controllers shall meet common requirements for gain and phase margins (6 dB, 45 deg).

The resulting parameter dependent controller

$$K_\rho = \left[\begin{array}{c|c} A_K(\rho, \dot{\rho}) & B_K(\rho) \\ \hline B_K(\rho) & D_K(\rho) \end{array} \right] \tag{5}$$

is synthesized solving a convex optimization problem [22].

The obtained controller therefore minimizes the upper bound on the induced L_2-norm of the interconnection in Fig. 1 with inputs $\begin{bmatrix} r & d_i & d_o \end{bmatrix}^T$ and outputs $\begin{bmatrix} z_e & z_u \end{bmatrix}^T$

$$P \overset{S}{=} \left[\begin{array}{c|ccc} A(\rho) & B_{11}(\rho) & B_{12}(\rho) & B_2(\rho) \\ \hline C_{11}(\rho) & D_{1111}(\rho) & D_{1112}(\rho) & 0 \\ C_{12}(\rho) & D_{1121}(\rho) & D_{1122}(\rho) & I \\ C_2(\rho) & 0 & I & 0 \end{array} \right]. \tag{6}$$

Assumptions necessary to solve this state feedback and observer problem (no full state feedback available) are described in [15].

As proven in [15], [21], an output feedback controller K that stabilizes the closed loop interconnection $G_{cl,\rho} = \mathscr{F}_{\mathscr{L}}(P,K)$ and guaranteed $\|G_{cl,\rho}\| < \gamma$ can be found if there exist symmetric positive definite matrix functions $X : \mathbb{P} \to \mathbb{R}^{n \times n}$ and $Y : \mathbb{P} \to \mathbb{R}^{n \times n}$ such that $\forall(\rho,\dot{\rho}) \in \mathbb{P} \times \dot{\mathbb{P}}$

$$\begin{bmatrix} X_\rho & \frac{1}{\gamma}I \\ \star & Y_\rho \end{bmatrix} \prec 0, \quad \begin{bmatrix} \Lambda_X - B_2 B_2^T & X_\rho C_{11}^T & \frac{1}{\gamma}(B_1 - B_2)D_{112\bullet}) \\ \star & -I & \frac{1}{\gamma}D_{111\bullet} \\ \star & \star & -I \end{bmatrix} \prec 0, \tag{7}$$

$$\begin{bmatrix} \Lambda_Y - C_2^T C_2 & Y_\rho B_{11} & \frac{1}{\gamma}(C_1^T C_2^T D_{11\bullet 2}) \\ \star & -I & \frac{1}{\gamma}D_{11\bullet 1}^T \\ \star & \star & -I \end{bmatrix} \prec 0 \tag{8}$$

where $\star$ denotes symmetric completion and

$$\begin{aligned} \Lambda_X(p,q) &:= X(A - B_2 C_{12})^T + (A - B_2 C_{12})X - \sum_{i=1}^{n_\rho} \left.\frac{\partial X}{\partial \rho_i}\right|_p \dot{\rho}_i \\ \Lambda_Y(p,q) &:= Y(A - B_{12}C_2)^T + (A - B_{12}C_2)Y - \sum_{i=1}^{n_\rho} \left.\frac{\partial X}{\partial \rho_i}\right|_p \dot{\rho}_i. \end{aligned} \tag{9}$$

As equation 9 depends also on the rate of change in the parameter, $\dot{\rho}$, for the search of the functional relations $X(\rho)$ and $Y(\rho)$ m$^{\text{th}}$ order polynomial base functions of the form

$$X(\rho) = X_0 + \rho_1 \cdot X_{11} + \rho_1^2 \cdot X_{12} + \dots + \rho_n{}^m X_{n,m} \tag{10}$$

are selected [22]. The choice of the base function parameters is up to the designer. It is useful to choose the base functions as simple as possible, as the number of unknowns in these functions correlates to the unknowns in the Linear Matrix Inequalities (LMIs) in equation 7 and increases therefore complexity of the problem. With the found solutions for $X(\rho)$ and $Y(\rho)$ a controller K_ρ in the form of equation 5 is calculated. For the calculations of the four controller matrices from $X(\rho)$ and $Y(\rho)$ it is referred to Sect. 4 in [22].

Design examples for LPV controllers in literature can be found in [14], [22]. The available `LPVTools MATLAB` toolbox [7] implements the solution to the LPV control problem in a similar way as described above.

3 Modeling and Control Design

3.1 Aircraft Model

The Cessna Citation II depicted in Fig. 2 is a research aircraft operated by the Delft University of Technology. The aircraft is equipped with a conventional reversible flight control system (FCS) providing a fix-geared link between the pilot's controls and the control surfaces. Furthermore, its autopilot uses electrical servos connected to the conventional controls. The aircraft was modified with a fly-by-wire system [23], which uses these autopilot servos as control actuators. In addition, a flight test instrumentation system [10] allowing data acquisition and logging is available.

The simulation model available was developed using the Delft University Aircraft Simulation Model and Analysis Tool (DASMAT) [19] and allows simulation and control design within the MATLAB / Simulink environment. The used DASMAT model was originally generated for a Cessna Model 500 Citation; nonetheless the modified simulation model shows good compliance with the Citation II [8]. The used aircraft model features a standard 6 Degree of Freedom (DOF) nonlinear equation with aerodynamic lookup table data based on [19]. The actuators were modeled as second order transfer functions according to [5]. The sensors are modeled as a combination of time delay, bias and noise. The basic flight control system is included and features a servo controller which is able to set the actuator positions commanded by the flight control laws.

In order to obtain an LPV model of the Citation II aircraft, the nonlinear model is trimmed and linearized at a grid of operating points. Thus, a model according to equation 1 is obtained. As scheduling variable, dynamic pressure

$$\bar{q} = \frac{\rho}{2}V^2 \tag{11}$$

is chosen, where ρ is air density and V true airspeed. For longitudinal and lateral dynamics, the LPV model of the full plant is fractioned into two models as for controller design it is appropriate to consider the two axes as decoupled [3].

Fig. 2 Cessna Model 550 Citation II Research Aircraft PH-LAB [9].

In the scheduling parameter, dynamic pressure $\bar{q}$ is considered in a range of $\bar{q} \in [2250, 6500]$ Pa, which corresponds to a range of true airspeeds from $76\,\mathrm{m\,s^{-1}}$ to $129\,\mathrm{m\,s^{-1}}$ at an altitude of 4,500 m (Flight Level (FL) 150)). The parameter rate is bounded to be within $\pm 500\,\mathrm{Pa\,s^{-1}}$. This corresponds to a rate of change in airspeed of approximately $7\,\mathrm{m\,s^{-1}}$ when at FL 450 with initial airspeed of $90\,\mathrm{m\,s^{-1}}$. For the controller development, an equally spaced parameter grid with 18 points was selected and verified against a denser grid of more than 50 points. Fig. 3 depicts the poles of the open loop plant 4×4 Linear Time Invariant (LTI) models of the aircraft at four equidistantly chosen grid points, namely dynamic pressure values of 2250, 3500, 5000 and 6500 Pa are shown. From the figure, the conjugate complex poles of SP mode can be read with frequencies ranging from 2 to 3 rad $\mathrm{s^{-1}}$ and a damping ratio of approximately 0.45. The Dutch Roll (DR) motion is located at a similar frequency range, but with a damping ratio of slightly less than 0.2 this mode is only poorly damped. The roll time constant t_r can be read to a range from 0.33 s at highest dynamic pressure to 0.5 s at the lowest dynamic pressure value. The Phugoid and Spiral poles have large time constants and are located near (0,0) in Fig. 3.
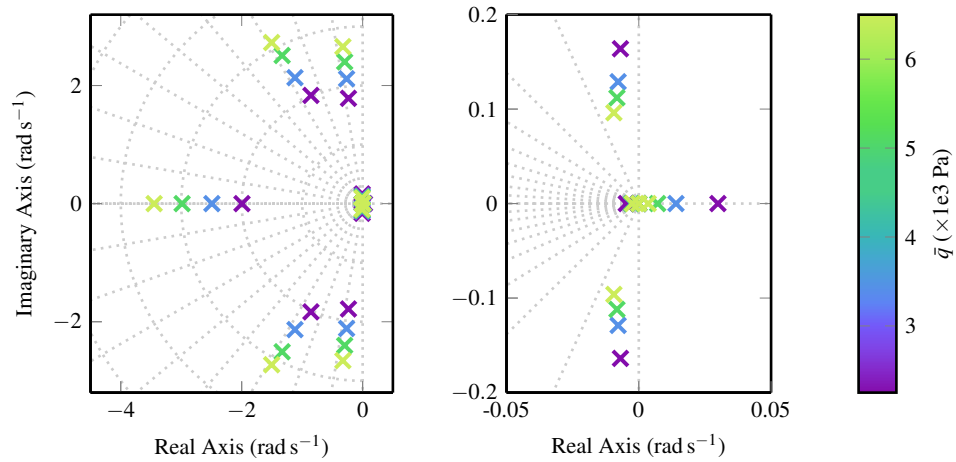
Fig. 3 Pole map of the open loop LTI models at 4 different values of $\bar{q}$, 4$^{\text{th}}$ order longitudinal and 4$^{\text{th}}$ order lateral model poles (left hand side: roll mode real valued poles, Dutch Roll only slightly damped and SP with higher damping ratio, right hand side: zoomed in, real valued Spiral mode which gets slightly unstable for lower airspeeds, Phugoid mode).

The following control design is carried out with the LPV models for longitudinal and lateral dynamics obtained here.

3.2 Longitudinal Control Laws

For the longitudinal control augmentation, two different reference variables were selected for control law design:

- **Load factor control** $n_{z,\text{cmd}}$, which commands the maneuver load factor of the aircraft set by the pilot's pitch control input. As the $n_{z,b}$ sensor measurement includes gravity, the feedback needs to be corrected by the aircraft's pitch and roll attitudes:

$$n_{z,\text{man}} = n_{z,\text{cg}} \frac{\cos(\Theta)}{\cos(\Phi)} \qquad (12)$$

  This corrected value $n_{z,\text{man}}$ results in a value of $1\,\text{g}$ independent of the aircrafts attitude and flight path.
- **Pitch rate control** q_{cmd}, where stick deflection is proportional to rate of pitch attitude change.

Both design approaches offer the comfort that a command input of 0 results in attitude hold behavior which is convenient for augmented flight. Therefore, both options relate neutral stick input to a $1\,\text{g}$ flight with pitch attitude hold. As the test aircraft is not equipped with an auto-throttle system, manual control of the throttle is mandatory to maintain an airspeed and dynamic pressure in the valid test envelope. In order to obtain a stable and controllable plant, control design uses only elevator input together with the SP model. Angle of attack and pitch rate are the states and load factor n_z is selected as additional plant output. As mentioned, due to a missing auto-throttle, the 4$^{\text{th}}$ order longitudinal model is uncontrollable. Therefore, Phugoid poles are not considered for the controller synthesis and only the 2$^{\text{nd}}$ order SP model is used. When integrating the controller into the full model, the result will be a Phugoid motion with two real poles of which one may be in the unstable region, but with a time constant larger than 30 seconds. This leads to the requirement of manual adjustment of thrust settings accordingly to avoid stall or overspeed regions of the envelope.

The limits of the controlled outputs shall be $\pm\,0.3\,\text{g}$ for load factor control and $\pm$ $5\,\text{deg s}^{-1}$ for pitch rate control. In this section, the design process for the maneuver load factor is depicted, thus $r = n_{z,\text{man}}$, being the tracking reference variable. The design for pitch rate control follows a similar scheme. The measured outputs are the load factor in body z-axis and the pitch rate of the aircraft. Design goals for the longitudinal motion are defined in [18] via the control anticipation parameter, as well as a minimum SP damping of $\zeta = 0.3$ and an optimal SP damping value of $\zeta = 0.7$.

The control anticipation parameter describes the relation of the immediate pitch acceleration to a control input and the 'stationary' load factor which will be the result of this maneuver. The control anticipation parameter (CAP) is defined as

$$\text{CAP} = \frac{\omega_{SP}^2}{n_{z,\alpha}}, \qquad (13)$$

where ω_{SP} is the SP frequency and $n_{z,\alpha}$ the (stationary) load factor resulting from a change in angle of attack. The value of $n_{z,\alpha}$ is characteristic for each aircraft, thus only ω_{SP} can be influenced. The CAP has an optimal value of one, which means the pilot is able to determine the amount of stick input needed for a certain load factor easily from the pitch acceleration $\dot{q}_0$ which is a direct result of an elevator deflection η, whereas the load factor n_z takes time to build up as it has two integral stages in between:

$$\eta \to \dot{q} \xrightarrow{\int} q \to \dot{\alpha} \xrightarrow{\int} \alpha \to n_z \tag{14}$$

In case of a CAP smaller than one, the pitch acceleration after a control input is low and the pilot will have the tendency of underestimating the stationary load factor, thus give higher pitch input as needed and overshoot the aimed load factor. The

Fig. 4 Control Anticipation Parameter (CAP) for the n_z control law throughout the flight envelope of the closed loop compared to the open loop (○). Additionally, the ideal CAP = 1 (– – –) and level 1 flying qualities region boundaries (– – –) according to [18] are depicted.
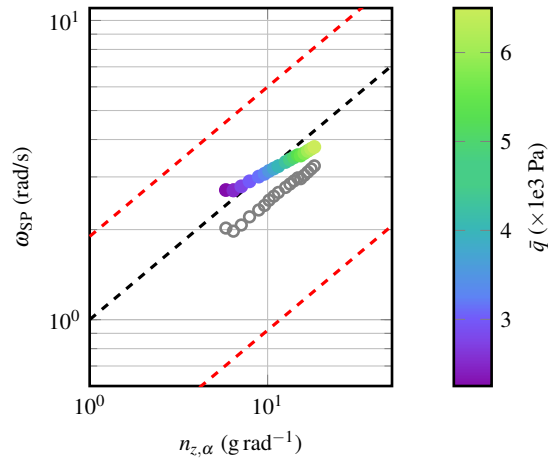
handling quality level 1 boundaries and results of the chosen controller design for load factor control can be seen in Fig. 4. As depicted, the resulting CAP is in the level 1 region close to the optimal value for the whole design envelope which was in this case achieved with a constant handling quality filter using a frequency of $1.75\,\text{rad}\,\text{s}^{-1}$ and a damping ratio of 0.8. The frequency responses for sensitivity, complementary sensitivity and reference tracking function are depicted in Fig. 5. From the right hand plot the maximum frequency for reference tracking can be read to $0.4\,\text{rad}\,\text{s}^{-1}$ and the left hand plot shows tracking behavior for the pitch rate command controller which maintains tracking behavior up to nearly $4\,\text{rad}\,\text{s}^{-1}$. Moreover, an increased SP damping ratio can be read from the pitch rate command pole plot in Fig. 6. The longitudinal controller features 12 states in case of the load factor command law and 9 states for the pitch rate command law. Fig. 7 shows the singular value plot of both control strategies. Both show integrating behavior until approximately $2\,\text{rad/s}$. Above, the curves open differ to varying open loop behavior with dynamic pressure and have a common roll off above or starting at about $20\,\text{rad/s}$.

The time domain results of the linear n_z command design are rise times smaller than 4 s for low and smaller than 2 s for high dynamic pressures. In terms of robustness, the multi-input-multi-output disk margin has a minimum at the upper end of the parameter envelope with values of 6.4 dB and 41 deg respectively, which can be considered as sufficient. The margins listed for the load factor control in Table 1 are a comparison of standard gain / phase / delay margins of loop cuts at sensor / actuator signal(s) with more significant disk margins and robustness margins used in [16]. The disk margin is computed according to [4] and values for the phase of the disk margin vs. the scheduling parameter of the controller are depicted in Fig. 8. The drop of the margins for the high dynamic pressure region calls for a careful flight testing at the end of the envelope. As the maneuverability of the experimental FCS is limited by relatively moderate power of the pitch servo, most maneuvers will be flown in a low dynamic pressure region.
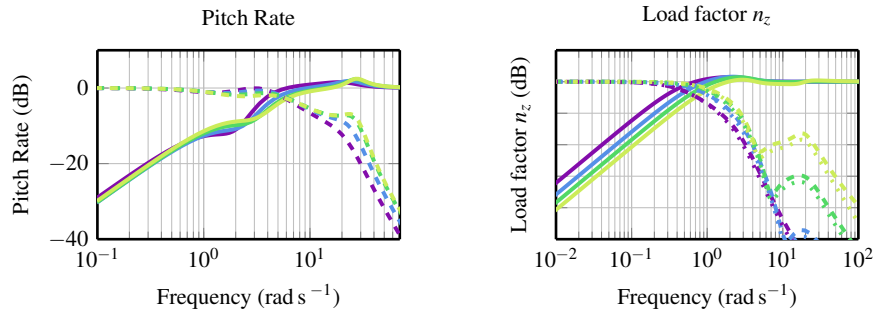
Fig. 5 Sensitivity function S (——), complementary sensitivity function T (- - -) and reference tracking function T_r (·····), depicted for the q_{cmd} controller on the left hand side and the $n_{z,cmd}$ control law on the right hand side. Both depicted for dynamic pressure values as seen in Fig. 4.

When looking at frequencies, it can be noted that the frequency of the disk margin drifts towards infinity, which makes it uncritical even in case of unintended exceed of the flight envelope.

Table 1 Minimum margins of the load factor controller.

Margin Type	Frequency (rad / s)	Value	
Gain Margin	247	13 dB	
Phase Margin	0.68	83 deg	
Delay Margin	1.0	1.44 s	
Disk Margin	117	11.8 dB	eq. 62 deg Phase Margin
MMIO[1]	0.81	6.4 dB	eq. 41 deg Phase Margin

[1] Multi-Input-Multi-Output Margin
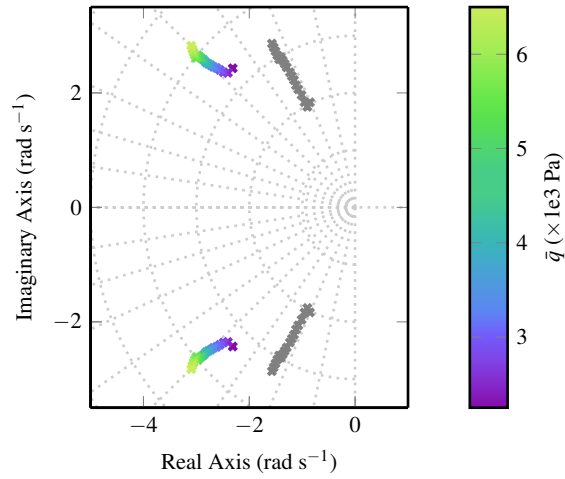
Fig. 6 Short period pole plot of the q_{cmd} controller (✖) and open loop Short Period poles (✳).
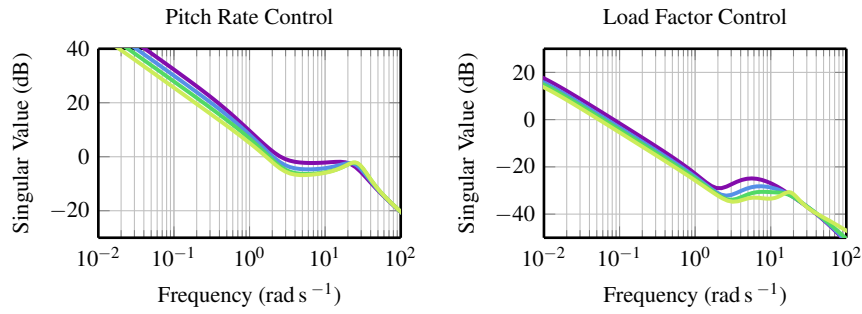

Fig. 7 Singular value plot of the pitch rate controller (left hand side) and load factor controller (right hand side) at 4 different dynamic pressure values (equally spaced over the envelope).
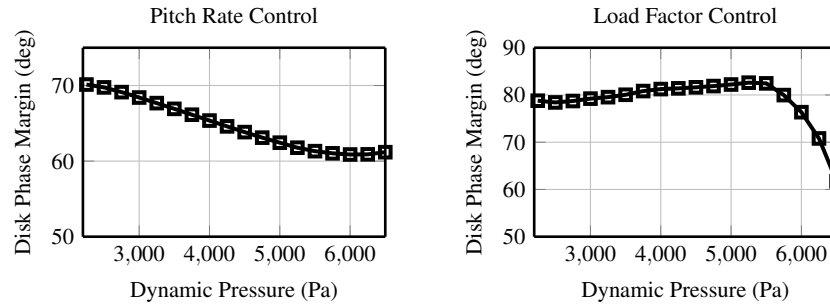

Fig. 8 Disk margin (phase) of the pitch rate controller (left hand side) and load factor controller (right hand side) w.r.t. scheduling parameter (dynamic pressure).

3.3 Lateral Control Laws

For the lateral inner loop the roll rate p and angle of side slip β are chosen as control variables. In the chosen setup, the experimental sidestick on the right hand pilot's seat allows the control of roll rate up to a bank angle of 27 deg, beyond constant stick input is needed for higher bank angles. The maximum bank angle of 35 deg shall never be exceeded and for a neutral stick the roll attitude will return to 27 deg. The aircraft is not equipped with a yaw input on the experimental FCS, thus the yaw axis can be assessed via differential thrust settings or slip inputs triggered by the flight test crew.

For the inner loop control laws designed in this section, flying quality specifications for lateral axis [18] request a maximum time of 2 s for a 30 deg bank angle change. Thus, a roll rate limit of $p_{\max} = 15$ deg s^{-1} is introduced to fulfill this requirement. The roll time constant t_r shall be less than one second, which allows a quick response to pilot's sidestick input. For the DR mode, specifications request a minimum damping of 0.08 and a minimum frequency of 0.4 rad s^{-1} as well as the product of damping and frequency to be at least 0.15 rad s^{-1}.

The handling quality filter for roll rate is chosen as a second order filter in the form of equation 4 with a frequency of $\omega_{SP} = 5$ rad s^{-1} and a damping of $\zeta = 0.9$, to provide tracking of commanded roll rate. The same form of filter, with a lower corner frequency, is chosen for the angle of sideslip channel. For both the performance weight on the tracking error is chosen as a transfer function with integrating behavior up to a frequency of 12 rad/s, which is sufficiently lower than the actuator bandwidth of 30 rad/s. The actuator weights are chosen with differentiating behavior above the actuator bandwidth. All other weights are chosen as constant. The resulting sensitivity and complementary sensitivity functions are depicted in Fig. 9. For both reference variables, nearly parameter independent behavior has been achieved which results in similar aircraft responses in roll axis over the whole envelope. Roll rate is tracked up to a frequency of 8 rad s^{-1} and angle of sideslip up to 1 rad s^{-1}, above this frequency tracking accuracy diminishes due to higher prioritized yaw damping. The lateral controller has a number of 20 internal states.
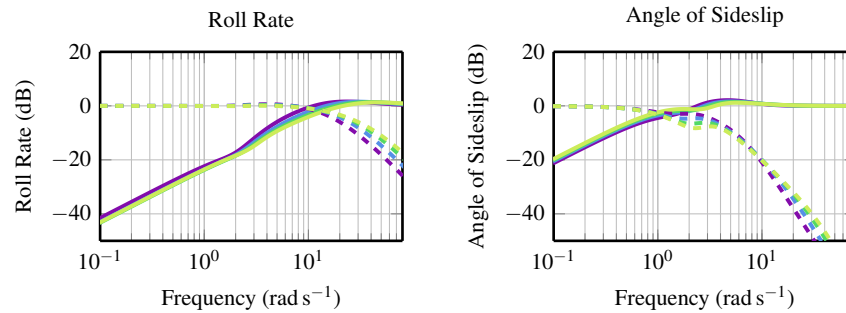
Fig. 9 Sensitivity function S (——) and complementary sensitivity function T (- - -) of the lateral dynamics.

Fig. 10 shows the closed loop poles of the controlled LPV system versus the poles of the uncontrolled LPV plant. According to the previously explained tracking behavior, it can be clearly seen that a unique roll time constant for the full envelope is generated. This ensures similar times for the build-up of roll rate independent of the dynamic pressure, thus the pilot can expect similar behavior of the aircraft's roll axis without considering the actual airspeed and altitude. Moreover, an increased damping of the DR motion is achieved when comparing the closed loop with open loop poles.
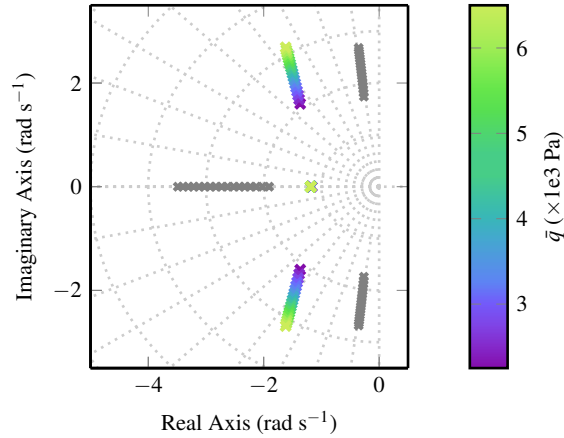

Fig. 10 Poles of lateral open loop (✳) and closed loop (✖). Dutch Roll shows increased damping ratio for the closed loop and roll time constant is clipped to only one value for the whole parameter envelope in closed loop.
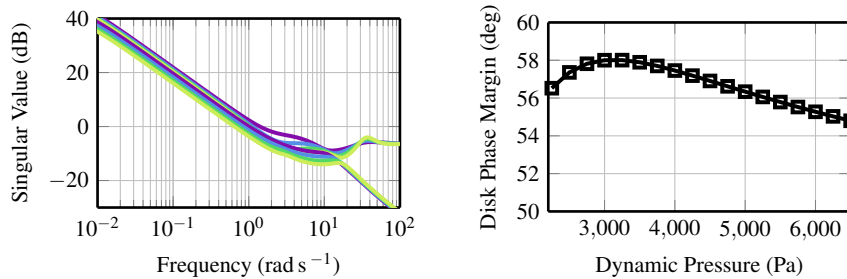
Fig. 11 Left hand side: Singular value plot of the lateral controller, displayed at 4 equidistantly spaced scheduling points. Right hand side: minimum disk margin (phase) of the lateral control loop w.r.t. scheduling parameter.

Furthermore, the left hand side of Fig. 11 depicts the singular values over frequency of the resulting LPV lateral inner loop controller. Up to the DR Frequency all curves show similar, integrating behavior whereas above this frequency, until about 10 rad/s the dependency on the value of the scheduling parameter can be seen in the controller gain. On the right hand side plot in Fig. 11, the phase of the minimal disk

margin of the lateral controller is depicted. For comparison of classical gain / phase margins and the robustness margin computations introduced in Sect. 3.2, the values shown in Table 2 are calculated. With a minimum of 4.2 dB, sufficient robustness even against simultaneous variations in all channels is ensured.

Table 2 Minimum Margins of the lateral control loop.

Margin Type	Frequency (rad / s)	Value	
Gain Margin (I[1])	1.38	11.5 dB	
Phase Margin (I)	0.45	73.8 deg	
Gain Margin (O[2])	1.72	10.8 dB	
Phase Margin (O)	0.47	70.2 deg	
Delay Margin (I/O)	1.72	0.54 s	
Disk Margin (I)	1.21	11.3 dB	(equals 59.5 deg Phase Margin)
Disk Margin (O)	1.31	10.0 dB	(equals 54.8 deg Phase Margin)
MMIO[3]	1.35	4.2 dB	(equals 26.8 deg Phase Margin)

[1] Minimum Margin on all input loop cuts [2] Minimum Margin on all output loop cuts [3] Multivariate Multi Input/Output Margin

4 Controller Verification

For verification of the designed control laws, an extensive simulation campaign to validate the controller is conducted which includes non-linear simulation on the DLR Robotic Motion Simulator. For controller verification, a set of maneuvers which includes a step-like commands and augmented flying by a test pilot is carried out. Additionally, changes in the operating point shall verify a smooth behavior of the controlled test aircraft later on.

The Institute of System Dynamics and Control's RMS [2] is used as a platform for flight test preparation via non-linear simulations. The RMS is a seven degree of freedom industrial robot, depicted in Fig. 12, which seats one person and can be equipped with aircraft controls and virtual reality glasses in order to provide the user with a real-time response in terms of accelerations, body rates and attitudes. The pilot input, given via sidestick and thrust levers, is processed in the main simulation model and its 6 DOF outputs are delivered as inputs to the RMS. Filtering algorithms ensure the gravity vector is always pointing in the direction of the stationary acceleration vector and higher frequency accelerations are depicted via translation and rotation of the gondola seen in Fig. 12. Visual information is provided to the user via virtual reality glasses and includes a cockpit view perspective of the flight trajectory as well as a primary flight display which can be customized with test rel-

Fig. 12 Robotic Motion Simulator at the DLR Institute of System Dynamics and Control [2].

evant parameters.

As the research platform used in flight does require discretization of the produced controller, also for the simulator experiments a continuous implementation is used which transmits and receives at a rate of 100 Hz.

At first, longitudinal axis is verified as longitudinal command is also needed during bank maneuvers. Fig. 13 shows a step in load factor command for the designed load factor command control law. The depicted measurement signal is the total body acceleration in z-axis direction at the center of gravity. As the delta in command shall be a pure maneuver load, the load factor demand needs to be scheduled with the cosine of current pitch attitude. The signals depicted are taken from the model's sensor outputs, thus sensor noise and air turbulence is included in the simulation results. As seen, the aircraft tracks the reference and has only very slight overshoots in pitch rate during capture of the second command step. When flown in the robotic motion simulator, attitude hold behavior results in smooth flight with no bumps or jolts despite the activated light air turbulence. Command provides satisfactory tracking although providing a slower response than the pitch rate command control law.

For lateral axis, roll time constant is compared for open and closed loop in Fig. 14. The plot shows step responses in the roll rate for two different operating points of 85 m/s and 110 m/s airspeed at the same altitude. The closed loop responses show the same slope as expected due to a fixed roll time constant for the whole parameter envelope. In contrast, the open loop curves show the expected behavior of a varying roll time constant at different airspeeds. Due to the given aileron step command, stationary roll rates differ for the open loop curves. Fig. 15 shows closed loop roll rate command for the same two airspeeds during a 5 s bank command and the occurring angle of sideslip.
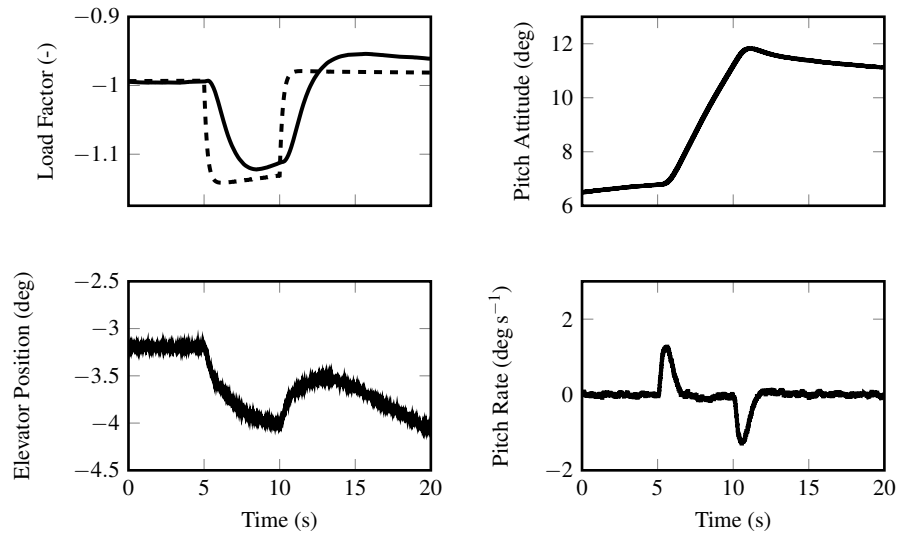
Fig. 13 Closed loop step response in longitudinal axis (━━━) to a load factor command of $\Delta n_z = 0.15\,\text{g}$ (━ ━ ━).
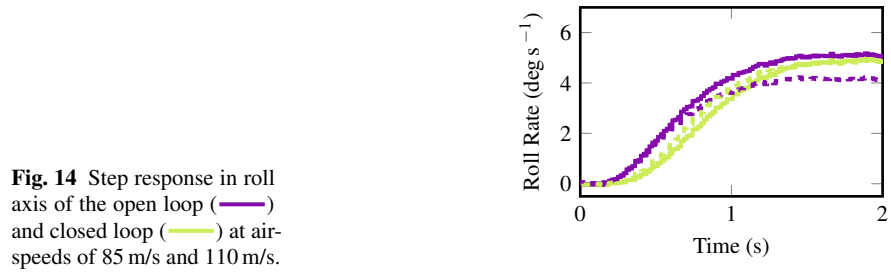
Fig. 14 Step response in roll axis of the open loop (━━━) and closed loop (━━━) at airspeeds of 85 m/s and 110 m/s.
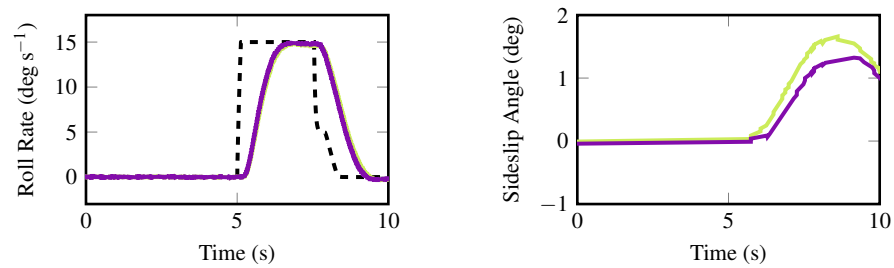
Fig. 15 Response lateral axis at airspeeds of 85 m/s (━━━) 110 m/s (━━━) at an altitude of 4500 m.

5 Conclusions

In this work a Linear Parameter Varying based flight control system has been developed for a CS 25 certified aircraft. The obtained flight controller has been validated through extensive simulations and will be validated in a flight test campaign shortly. The results until now show the successful implementation of the controller design tool-chain, including controller design itself, (non-linear) simulation based verification which proves flight readiness of the derived control laws. In detail, the flight control algorithms which have been presented meet the previously set design goals in tracking behavior, robustness against model uncertainties and disturbance rejection.

Following this simulation based verification, the controller will be assessed onboard a research aircraft shortly. Additionally to the performance validation of the control laws, the included scheduling of the controller with respect to dynamic pressure will be demonstrated within the flight testing.

Acknowledgement

References

[1] P. Apkarian, P. Gahinet, and G. Becker, "Self-scheduled H$_\infty$ control of linear parameter-varying systems: A design example," *Automatica*, vol. 31, no. 9, pp. 1251–1261, Sep. 1995.

[2] T. Bellmann, J. Heindl, M. Hellerer, R. Kuchar, K. Sharma, and G. Hirzinger, "The DLR robot motion simulator part I: Design and setup," in *IEEE International Conference on Robotics and Automation*, May 2011.

[3] R. Brockhaus, W. Alles, and R. Luckner, *Flugregelung*, 3., neu bearb. Aufl. Berlin Heidelberg: Springer-Verlag Berlin Heidelberg, 2011.

[4] I. P. D. Bates, *Robust Multivariable Control of Aerospace Systems*. IOS PR, Jun. 11, 2002, 212 pp.

[5] S. den Braven and J. Verspay, "Identification of the servo actuated flight control system of the Cessna Citation II," National Aerospace Laboratory NLR, 1994.

[6] F. Grondman, G. Looye, R. O. Kuchar, Q. P. Chu, and E.-J. van Kampen, "Design and flight testing of incremental nonlinear dynamic inversion-based control laws for a passenger aircraft," in *AIAA Guidance, Navigation, and Control Conference*, Jan. 2018.

[7]   A. Hjartarson, P. Seiler, and A. Packard, "LPVTools: A toolbox for modeling, analysis, and synthesis of parameter varying control systems," *IFAC-PapersOnLine*, vol. 48, no. 26, pp. 139–145, 2015.

[8]   M. A. van den Hoek, C. C. de Visser, and D. M. Pool, "Identification of a Cessna Citation II model based on flight test data," in *Advances in Aerospace Guidance, Navigation and Control*, Springer International Publishing, Dec. 2017, pp. 259–277.

[9]   P. Lu and E.-J. van Kampen, "Aircraft inertial measurement unit fault identification with application to real flight data," in *AIAA Guidance, Navigation, and Control Conference*, Jan. 2015.

[10] A. Muis, J. Oliveira, and J. A. Mulder, "Development of a flexible flight test instrumentation system," 2006.

[11] G. Papageorgiou, K. Glover, G. D'Mello, and Y. Patel, "Taking robust LPV control into flight on the VAAC harrier," in *Proceedings of the 39th IEEE Conference on Decision and Control (Cat. No.00CH37187)*.

[12] G. Papageorgiou and K. Glover, "Design of a robust gain scheduled controller for the high incidence research model," in *Guidance, Navigation, and Control Conference and Exhibit*, American Institute of Aeronautics and Astronautics, Aug. 1999.

[13] H. Pfifer, *LPV/LFT Modeling and its Application in Aerospace*, 1. Aufl., ser. Luftfahrt. München: Dr. Hut, 2013.

[14] H. Pfifer and S. Hecker, "Lpv controller synthesis for a generic missile model," in *IEEE International Conference on Control Applications and CCA and IEEE Multi-Conference on Systems and Control and MSC*, Piscataway, NJ, 2010.

[15] F. Saupe, H. Werner, U. Weltin, and E. Kreuzer, *Linear Parameter Varying Control Design for Industrial Manipulators*, ser. Fortschritt-Berichte VDI Reihe 8, Mess-, Steuerungs- und Regelungstechnik. Düsseldorf: VDI-Verl., 2013, vol. 1223.

[16] A.-K. Schug, P. Seiler, and H. Pfifer, "Robustness margins for linear parameter varying systems," Eng, *AerospaceLab Journal*, vol. Issue 13, ISSN: 2107-6596, 2017.

[17] S. Skogestad and I. Postlethwaite, *Multivariable Feedback Control: Analysis and Design*, 2. ed. Chichester: Wiley, 2005.

[18] US Department of Defense, *MIL-F-1797C: Flying Qualities of Piloted Aircraft*, 1997.

[19] C. A. A. M. van der Linden, *Dasmat-Delft University Aircraft Simulation Model and Analysis Tool: A Matlab, Simulink Environment for Flight Dynamics and Control Analysis (Series 03 - Control and Stimulation , No 03)*. Delft Univ Pr, 1998.

[20] C. Weiser, D. Ossmann, and M. Heller, "In-flight validation of a robust flight controller featuring anti-windup compensation," in *Atmospheric Flight Mechanics Conference*, Jun. 2018.

[21] F. Wu, "Control of linear parameter varying systems," PhD thesis, University of Calicfornia, University of California, Berkeley, 1995.

[22] F. Wu, X. H. Yang, A. Packard, and G. Becker, "Induced L_2-norm control for LPV systems with bounded parameter variation rates," *International Journal of Robust and Nonlinear Control*, vol. 6, no. 9-10, pp. 983–998, Nov. 1996.

[23] P. Zaal, D. Pool, A. in 't Veld, F. Postema, M. Mulder, M. van Paassen, and J. Mulder, "Design and certification of a fly-by-wire system with minimal impact on the original flight controls," in *AIAA Guidance, Navigation, and Control Conference*, Aug. 2009.